# Numeical Simulation for the Turbulent Flow through Hydroturbine Components

Byeong Rog SHIN, Institute of Fluid Science, Tohoku University, Sendai 980-8577, Japan
E-mail: shin@ifs.tohoku.ac.jp http://www.ifs.tohoku.ac.jp

This paper presents a development of computational code for solving complex flow in turbomachinery. Using this code, a numerical study investigating a three-dimensional turbulent flow through a Francis turbine including spiral casing and turbine runner, where the flow is dominantly characterized by swirling flow accompanying unsteadiness is performed. This study aims at the improvement of performance characteristics for the turbine through optimal design. In order to implement the numerical simulation, the incompressible Navier-Stokes Equations are solved using an artificial compressibility method based on the third-order Runge-Kutta finite-volume method applying Roe's flux difference splitting scheme with TVD MUSCL approach and LES method for the subgrid scale turbulences. The predicted results were compared with those of measurements on the velocity distribution at a couple of places of inlet and outlet of the turbine runner. The agreement between the present predictions and measurements is quite good at most locations. It indicates the validity of the present code. Detailed observations of turbulent internal flows in hydraulic turbine of the spiral casing and the runner are made.

## 1. Introduction

Hydroelectric power being revaluated these days is a clean ecoenergy. From the view point of efficient use of this hydroenergy and hydroelectric power facilities, it is highly desired that the hydromachines and their equipments should have the wide operating range and their high performance characteristics, and minimize the hydraulic loss. Energy losses taking place in all the hydraulic components of turbomachinery mainly come from flow separation, secondary flow, profile drag, seal leakage and wall friction loss.

In order to respond to above requirements, a better understanding of the flow through the turbomachine components is important matter. In the hydraulic turbine, it is indispensable to make clear the flow characteristics around blades of the distributor and runner, which are fundamental components to govern the performance of turbines. From this reason, many studies to analysis flows related to the spiral casing [1,2], runner[3] and draft tube [4,5] of hydroturbines[6,7] have been made. At the GAMM Workshop in Lausanne[8], a realistic incompressible flow field in a Francis turbine had been chosen and studied. The majority of methods used in numerical predictions of the workshop is artificial compressibility method with integration of Euler equations of motion. Practically, the Euler equation model has been widely used among the designers of turbomachinery. However, Euler equation model is limited in its ability to predict the loss, efficiency and a lot of flow phenomena associated with turbulent and separating flows. Therefore, recently intensive efforts to develop Navier-Stokes codes which can predict turbulent flow have been devoted. Upto date as a turbulent model estimable the turbulence, $k$-$\varepsilon$ turbulence model has been utilized to analyze such a turbulent flow. Navier-Stokes analysis applying $k$-$\varepsilon$ turbulence model, however, often encounters the difficulty to represent the complex behavior of turbulent viscous flows in very complicated flow fields such as the Francis turbine, and to simulate flow unsteadiness because $k$-$\varepsilon$ model is a time-average technique and contains many model coefficients to be calibrated, so that it is incapable accurate simulation of the production and shedding of unsteady vortices.

At the present, fortunately, thanks to the rapid progress of the available computer ability, it has become possible to make an accurate analysis for practical three-dimensional (3-D) turbulent flows by applying large eddy simulation (LES) method[9,10]. The Navier-Stokes solver with LES method is considered as the most advanced computational fluid dynamics tool available, because the LES method can directly calculate all of the large scale turbulent eddies as functions of space and time, and only small eddies below the grid size are modeled. Lately, the authors have presented a study of LES analysis[11] for 3-D turbulent flow through a Francis turbine by using a multi-zone finite-volume method with MacCormack's predictor-corrector method and the weakly compressible flow model by Song and Yuan[12].

In the present paper, a development of efficient computational code for solving complex flow in turbomachinery is made by using an artificial compressibility method. It is based on the third-order Runge-Kutta finite-volume method applying Roe's flux difference splitting scheme[13] with TVD MUSCL approach[14] and LES method[15] for the subgrid scale turbulences. And a further investigation of turbulent flow in the Francis turbine spiral casing and runner is implemented. The predicted results are compared with those of LDV measurements[11] on the velocity distribution at a couple of locations between wicket gates and turbine runner to assess the validity of the present code as a efficient design tool for the hydroturbine.

## 2. Fundamental Equations

### 2.1 Fundamental Equations and LES Method

The hydraulic flow can be characterized as fully 3-D non-linear, viscous flow with laminar and turbulent regions. Also this flow with a highly time-dependent flow such as hydraulic transients and hydroacoustics presents the compressible flow characteristic at small Mach number. In the present study an application of an artificial compressibility method is made to predict such hydraulic flow. The governing equations for incompressible flow can be written as using the artificial compressibility parameter, $\beta$

$$\frac{\partial \boldsymbol{q}}{\partial t} + \frac{\partial \boldsymbol{E}}{\partial \boldsymbol{x}} = \boldsymbol{f} \tag{1}$$

where

$$\boldsymbol{q} = \begin{bmatrix} p \\ u \\ v \\ w \end{bmatrix},$$

$$\boldsymbol{E} = \begin{bmatrix} \beta u & \beta v & \beta w \\ uu + \tilde{p} - \tilde{\tau}_{xx} & uv - \tilde{\tau}_{xy} & uw - \tilde{\tau}_{xz} \\ uv - \tilde{\tau}_{yx} & vv + \tilde{p} - \tilde{\tau}_{yy} & vw - \tilde{\tau}_{yz} \\ uw - \tilde{\tau}_{zx} & vw - \tilde{\tau}_{zy} & ww + \tilde{p} - \tilde{\tau}_{zz} \end{bmatrix},$$

$\tilde{a} = a/\rho$, $\rho$ and $\nu$ are the density and kinematic viscosity. The symbols $p$, $\boldsymbol{u}(u, v, w)$ and $\boldsymbol{f}$ represent pressure, velocity and external force vector, respectively.

In the turbulent flow computation, LES method for the subgrid scale (SGS) turbulences is applied by adding the SGS stress term of $-\overline{u_i^{'} u_j^{'}}$ to the viscous terms of $\tau_{ij}$ in Eq.(1). In the present study, SGS turbulence model by Smagorinsky[15] is used as

$$-\overline{u_i^{'} u_j^{'}} = \nu_t \left( \frac{\partial u_i}{\partial x_j} + \frac{\partial u_j}{\partial x_i} \right) \tag{2}$$

where,

$$\nu_t = (C_s \Delta)^2 \sqrt{(2 S_{ij} S_{ij}}, \quad S_{ij} = \frac{1}{2} \left( \frac{\partial u_i}{\partial x_j} + \frac{\partial u_j}{\partial x_i} \right) \tag{3}$$

and $\Delta$ is the grid size, $C_s$ is the SGS coefficient.

For the flow through runner, the rotating coordinate system represented by the relative velocity is used. In this case, the force vector in Eq.(1) can be written as, with $\omega$ of the rotational speed around the $z$-direction (axial direction)

$$\boldsymbol{f} = [0,\ 2\omega v + \omega^2 x,\ -2\omega u + \omega^2 y,\ 0]^T \tag{4}$$

The governing equation (1) is solved by finite-volume method. To apply the finite-volume method, Eq.(1) is integrated and averaged over an arbitrary finite volume $\Delta V$, and then converted to the followings by using the divergence theorem.

$$\frac{\partial \bar{\boldsymbol{q}}}{\partial t} = -\frac{1}{\Delta V} \int_S \boldsymbol{n} \cdot \boldsymbol{E} ds + \bar{\boldsymbol{f}} \tag{5}$$

where, symbol $\boldsymbol{n}$ is unit outward normal vector on the bounding surface $S$ and the bar represents a volume averaged value. Also, to take account of near wall effects, the van Drist wall-damping function $f_d$ $(= 1 - \exp(-y^+/A^+))$ was imposed on $\nu_s$ in Eq.(3) with empirical coefficient $A^+$ of 26.

### 2.2 Time Integration

For numerical integration, Eq.(5) is discretized using a three-step Runge-Kutta explicit method with $L(\boldsymbol{q}) = \partial \boldsymbol{E}/\partial \boldsymbol{x} - \boldsymbol{f}$.

$$\begin{aligned} \boldsymbol{q}^{(1)} &= \boldsymbol{q}^{(n)} - \Delta L(\boldsymbol{q}^{(n)}) \\ \boldsymbol{q}^{(2)} &= \frac{3}{4}\boldsymbol{q}^{(n)} + \frac{1}{4}\{\boldsymbol{q}^{(1)} - \Delta L(\boldsymbol{q}^{(1)})\} \\ \boldsymbol{q}^{(n+1)} &= \frac{1}{3}\boldsymbol{q}^{(n)} + \frac{2}{3}\{\boldsymbol{q}^{(2)} - \Delta L(\boldsymbol{q}^{(2)})\} \end{aligned} \tag{6}$$

### 2.3 Space Discretization

The second-order central-difference is basically used for the space derivatives. However, for the convection term on the left-hand side of Eq.(1) the higher-order upwind difference scheme is applied to solve the high Reynolds number flow with accuracy and stability. A simple one-dimensional equation is considered to explain the upwind schemes as

$$\frac{\partial u}{\partial t} + \frac{\partial f(a, u)}{\partial x} = \frac{\partial u}{\partial t} + a \frac{\partial u}{\partial x} = 0 \tag{7}$$

where $a(u) = \partial f/\partial u$ is the propagating speed of waves or the transport speed of the convection term. The discretized equation of Eq.(7) can be generally written in the conservation form

$$\begin{aligned} u_i^{n+1} &+ \lambda\theta(\hat{f}_{i+1/2} - \hat{f}_{i-1/2})^{n+1} \\ &= u_i^n - \lambda(1 - \theta)(\hat{f}_{i+1/2} - \hat{f}_{i-1/2})^n \end{aligned} \tag{8}$$

where $\lambda = \Delta t/\Delta x$, $0 \leq \theta \leq 1$, and $\hat{f}$ is the numerical flux function as $\hat{f}_{i+1/2} = a_{i+1/2}(u_i + u_{i+1})/2$ in the case of the second-order central-difference scheme.

The numerical function $\hat{f}_{i+1/2}$ can be written in the Roe's flux difference splitting method[13] with the higher-order TVD MUSCL scheme as

$$\begin{aligned} \hat{f}_{i+1/2} = \frac{1}{2} \Big[ & f(u^L_{i+1/2}) + f(u^R_{i+1/2}) \\ & - |a_{i+1/2}|(u^R_{i+1/2} - u^L_{i+1/2}) \Big] \end{aligned} \tag{9}$$

where, $a_{i+1/2}$ are estimated by the Roe's averaging and

$$\begin{aligned} u^L_{i+1/2} = u_i + \frac{1}{4} \{ & (1 - \kappa) D^+ u_{i-1/2} \\ & + (1 + \kappa) D^- u_{i+1/2} \}, \end{aligned} \tag{10}$$

$$\begin{aligned} u^R_{i+1/2} = u_{i+1} - \frac{1}{4} \{ & (1 - \kappa) D^- u_{i+3/2} \\ & + (1 + \kappa) D^+ u_{i+1/2} \}, \end{aligned} \tag{11}$$

$$\begin{aligned} D^+ u_{i-1/2} &= \mathrm{minmod}(\Delta u_{i-1/2}, b\Delta u_{i+1/2}), \\ D^- u_{i+1/2} &= \mathrm{minmod}(\Delta u_{i+1/2}, b\Delta u_{i-1/2}), \\ D^- u_{i+3/2} &= \mathrm{minmod}(\Delta u_{i+3/2}, b\Delta u_{i+1/2}), \\ D^+ u_{i+1/2} &= \mathrm{minmod}(\Delta u_{i+1/2}, b\Delta u_{i+3/2}). \end{aligned}$$

Here, the minmod function are determined by

$$\mathrm{minmod}(x, y) = \mathrm{sign}(x)\max[0, \min\{|x|, y\mathrm{sign}(x)\}] \tag{12}$$

And, $\Delta u_{i+1/2} = u_{i+1} - u_i$. The parameter $\kappa$ is a linear combination parameter determined by the range of $-1 \leq \kappa \leq 1$, and it has an effect on the accuracy of Eqs.(10) and (11). Through the Taylor expansion, we know that the TVD schemes of Eqs.(10) and (11) has a third-order accuracy at $\kappa = 1/3$ and it becomes a second-order scheme at the other values of $\kappa$. On the other hand, the slope of the flux in the minmod function of Eq.(12) is controlled by the limiter $b$. The range of $b$, $1 \leq b \leq (3 - \kappa)/(1 - \kappa)$, is determined by the condition of TVD stable.

### 2.4 Boundary Conditions

3-D turbulent flows through a Francis turbine with specific speed of $N_S = 210$ (m,kW,rpm) are calculated. The present turbine includes three basic units of spiral casing containing 20 wicket gates and 20 stay-vanes,

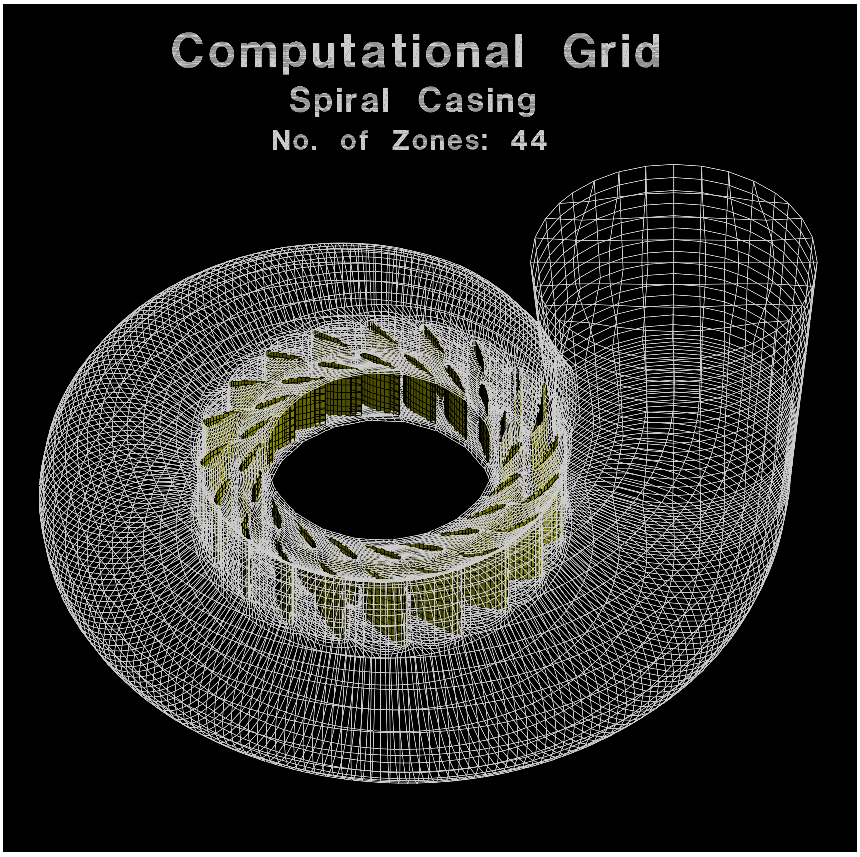


Fig.1: Computational grid for spiral casing

turbine runner having 13 blades with inlet diameter $D$ of $328.8mm$ and draft tube consisted of an inlet cone, an elbow and squared outlet sections with a center pier. The turbulent flow through the full model of spiral casing and draft tube is simulated. In the runner, however, the one and half partial flow passage among 13 passages is considered in the present study.

The flows through each of the basic units are computed separately, but the boundary conditions on the inlet of runner and draft tube are imposed using the result on the outlet from the computation of spiral casing and runner, respectively. At the casing entrance, a $1/7th$-power law velocity profile and zero pressure gradient are assumed. At the downstream boundary, the Neumann conditions are imposed. The no-slip condition is applied to all solid boundary. The three units consist of multi-zone, and boundary fitted computation grids generated by using the elliptic equation. $\rho c^2$ is chosen for $\beta$ in Eq.(1) by using the linear acoustic approximation with the sound speed $c$, and $C_s$ of 0.1 is used in Eq.(3).

## 3. Numerical Results

A numerical simulation for turbulet internal flow of the spiral casing and turbine runner is performed with a computational grid shown in Figs.1 and 2 which show a typical view of the total flow field of spiral casing and runner partitioned into 44 and 5 zones, respectively. In order to impose the appropriate boundary condition at the exit of wicket gates, the computational domain was extended one more zone downstream corresponded the whole water passage of runner chamber.

Figures 3(a) and (b) show a comparison of radial velocity ($U_r$) and tangential velocity ($U_\theta$) profiles at several positions of the runner inlet section of $1.2D$ and 192° from starting point of spiral. In these figures, "Runner" represents numerical results obtained from runner computation at one pitch space of runner blade. Also, the results obtained from the computation of spiral casing were presented by "Casing". The agreement between the present predictions and LDV measurements[11] is quite good at most locations. Especially, the tendency of $U_r$ near the band of runner is excellently predicted. The tangential components of velocity predicted from spiral casing in Fig.3(b), however, are somewhat different from experiments. These discrepancies are considered to be due to the separate implementation of computation in spite of the region to be strongly interacted by rotation of runner, in which $U_\theta$ is dominant rather than $U_r$. It implies a necessity of computation for a unified model with the spiral casing and runner.

The tangential velocity profiles at two linear directions of runner outlets are shown in Figs.4(a) and (b), where the directions are located respectively at 80° and 20° from starting point of spiral. $D_b$ is radial direction normalized by outlet diameter of turbine runner. Detailed measuring points are referred to Ref.[11]. The two results from measurement and LES are in good agreement even though the outlet is the region showing much more complicated flow phenomena than that of the runner inlet in Fig.3. Especially, the tendency of the velocity profiles with the radius is well captured. It is indicated that the present LES analysis by TVD MUSCL approach has a high reliability and to be a useful tool for designing of the turbomachinery.

Figure 5 shows instantaneous velocity and pressure fields near vanes and scroll surfaces at the 80% wicket gate opening. Figure 5(a) represents velocity distribution and stream traces and Fig.5(b) indicates surface

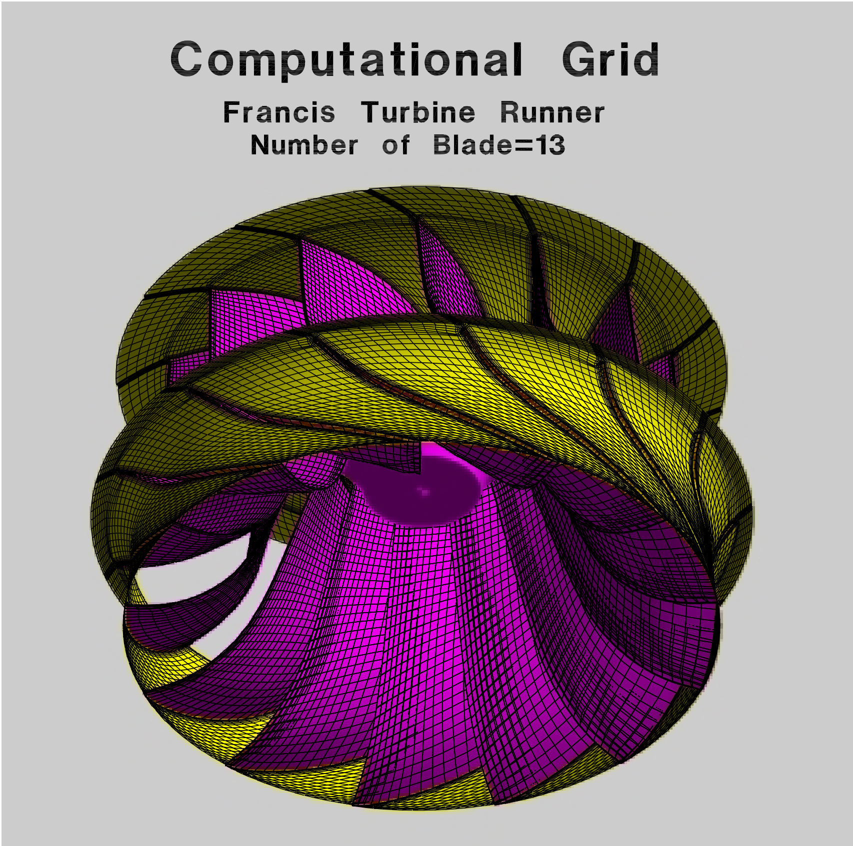


Fig.2: Computational grid for turbine runner

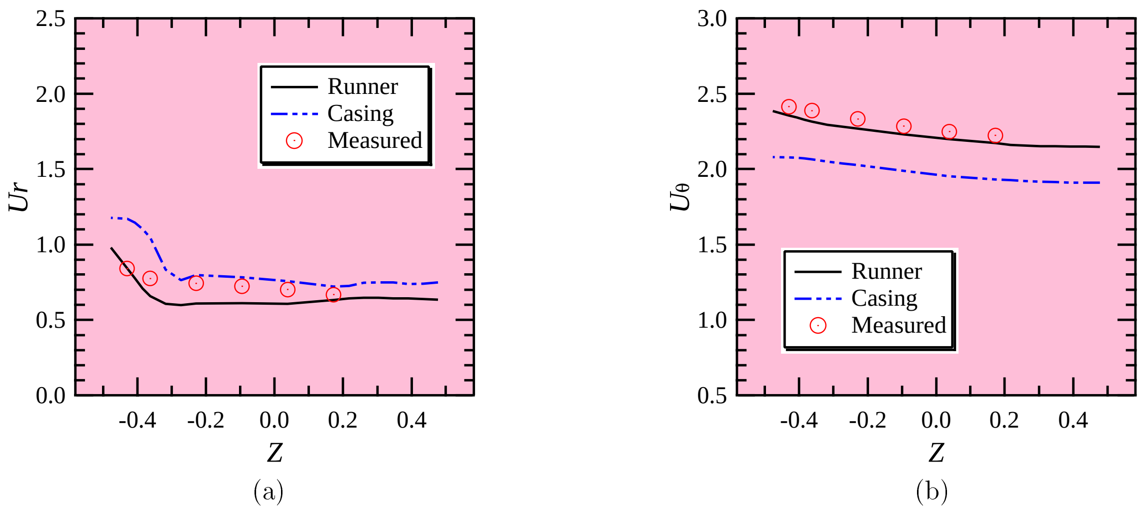


Figure 3: Comparison of velocity profiles with LDV measurements at runner inlet: (a) Radial velocity, $U_r$ and (b) Tangential velocity, $U_\theta$

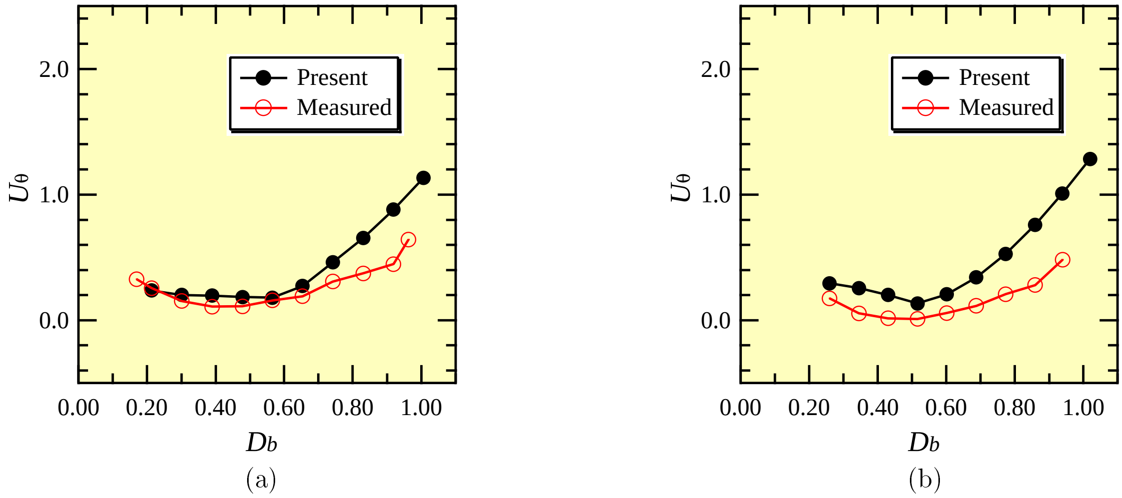


Fig.4: Comparison of tangential velocity profiles with LDV measurements at runner outlet: (a) at 80° and (b) at 20° from starting point of spiral

pressure and streamlines. In these figures, it can be seen that there exists a periodical unsteady swirling flow with three velocity and pressure peaks along the circumferential direction $\theta$, even though the time averaged flow is shown a typical monotonous down stream flow pattern of cascades not shown here. It is considered that these kind of unsteady flow phenomena are due to the mutual interaction between components containing the scroll, stay-vanes and wicket gates. These phenomena can be captured only by the computation of full 3-D domain flow model including the components, and lead to the vibration, noise and, consequently, a drop in performance of the turbine.

Figure 6 shows the computed time-averaged relative velocity magnitude and pressure distributions on the solid surfaces of the turbine runner at the maximum efficiency point. It is observed that the flow approximately has a direction of meridian on the suction side and it flows downward with a cross-flow from crown to band near the leading edge on the pressure side. The flow pattern seems reasonable at design condition and no separation appears. On the other hand, relatively low pressure is distributed near the band on this surface. On the pressure side the pressure decreases gradually toward downstream. Typical internal flow patterns through Francis turbine runner can be understood from these figures.

## 4. Conclusions

A development of computational code for solving complex turbulent flow in turbomachinery is presented. And a numerical study investigating 3-D turbulent flow through a Francis turbine including spiral casing and turbine runner is carried out to aim at an improvement of performance characteristics.

The incompressible flow equations of hydraulic turbine are solved by using an artificial compressibility method based on the third-order Runge-Kutta multizone finite-volume method applying a TVD MUSCL scheme and LES method for the subgrid scale turbulences. Two basic units of spiral casing and turbine runner are computed separately but the upstream boundary condition of runner is imposed by outlet flow conditions calculated at spiral casing.

From the 3-D full flow model computation for spiral casing, the flow unsteadiness and wicket gate-stay vane interaction could be investigated, and it gives information for advanced design of the physical model. In the comparison of predicted results with those of experiments on velocity profiles at the inlet and outlet regions of runner, they agree well with each other at most locations, except that the tangential components from the spiral casing are somewhat under predicted. Also, some observations of velocity and pressure distributions in two basic units are presented. It is indicated that the present LES analysis by Runge-Kutta explicit TVD MUSCL scheme is reasonable and reliable sufficiently, so that it is to be a useful tool for designing the turbomachinery with the high performance required.

## References

[1] Shyy, W. and Vu, T.C., ASME J. of Fluids Engng, **115** (1993), p.103

[2] Suzuki, T. et al., *ASME Paper*, FED-Vol.120 (1991), pp.105-111

[3] Avellan, F. et al., *Notes on Numerical Fluid Mechanics*, Vol.39 (1993), pp.33-53

[4] Agouzoul, M. et al., ASME J. of Fluids Engng, **112** (1990), p.257

[5] Vu, T.C. and Shyy, W., ASME J. of Fluids Engng, **112** (1990), p.5

[6] Ecer, A. and Akay, U., *SAE Tech. Paper Series* No.881274 (1988)

[7] Riedelbauch, S. et al., *Proc. 17th IAHR Symp.*, Vol.1 (1994), pp.353-364

[8] Sottas, G. and Ryhming, I.L., *Notes on Numerical Fluid Mechanics*, Vieweg, Vol.39, (1993)

[9] Song, C.C.S. et al., *Proc. 18th IAHR Symp.*, Valencia (1996), pp.267-276

[10] Song, C.C.S. et al., *Proc. 18th IAHR Symp.*, Valencia (1996), pp.277-283

[11] Shin, B.R. et al., *Proc. Int. Conf. on Fluid Engng, JSME Centennial Grand Congress*, Vol. III (1997), pp.1753-1758

[12] Song, C.C.S. and Yuan, M., ASME J. of Fluids Engng, **110** (1988), pp.441-445

[13] Roe, P.L., J. of Comput. Phys., **43** (1981), pp.357-372

[14] van Leer, B., J. of Comput. Phys., **32** (1979), pp.101-136

[15] Smagorinsky, J., Mon. Weath. Rev., **91** (1963), pp.99-164

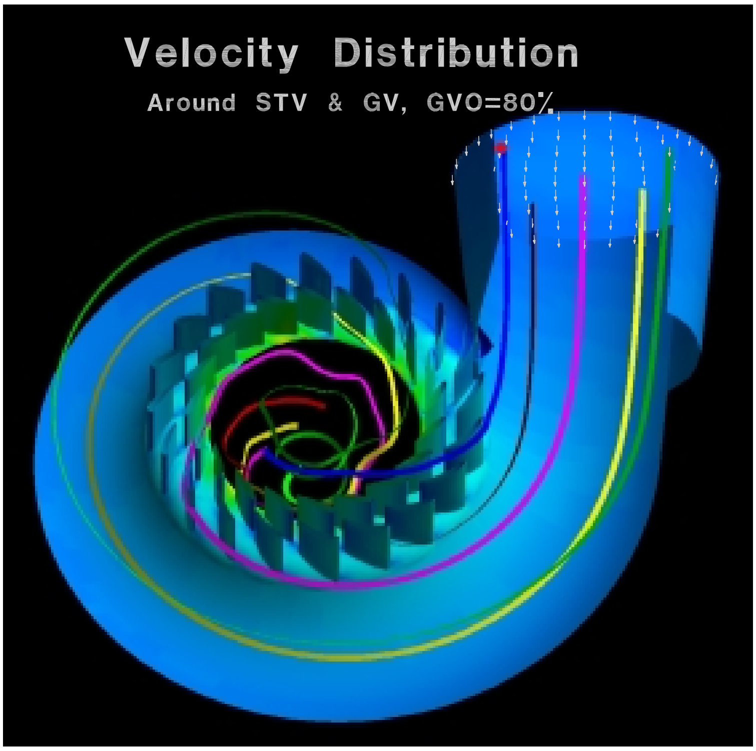


(a)

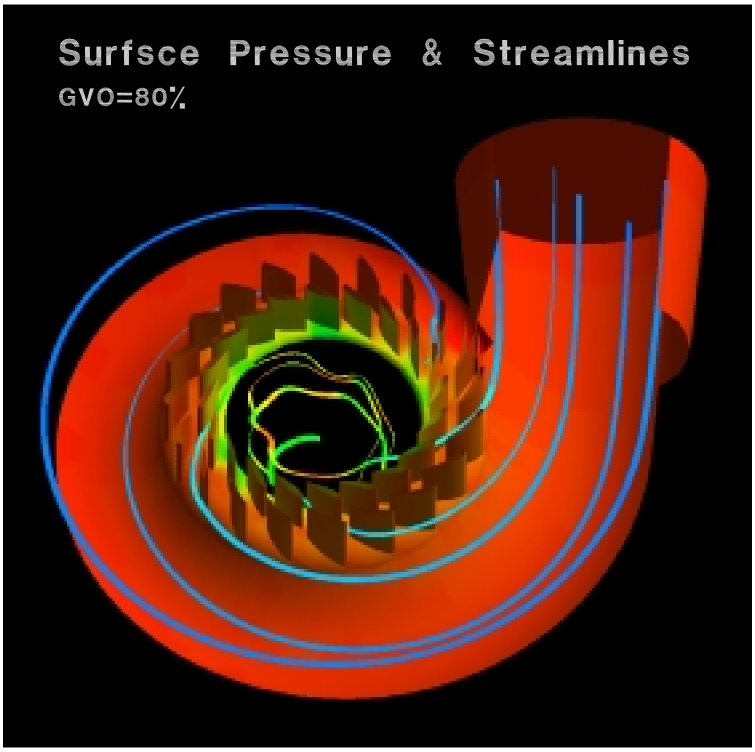


(b)

Fig.5: Instantaneous velocity and pressure distrubution at 80% wicket gate opening: (a) Velocity distrubution and stream traces and (b) Surface pressure and streamlines

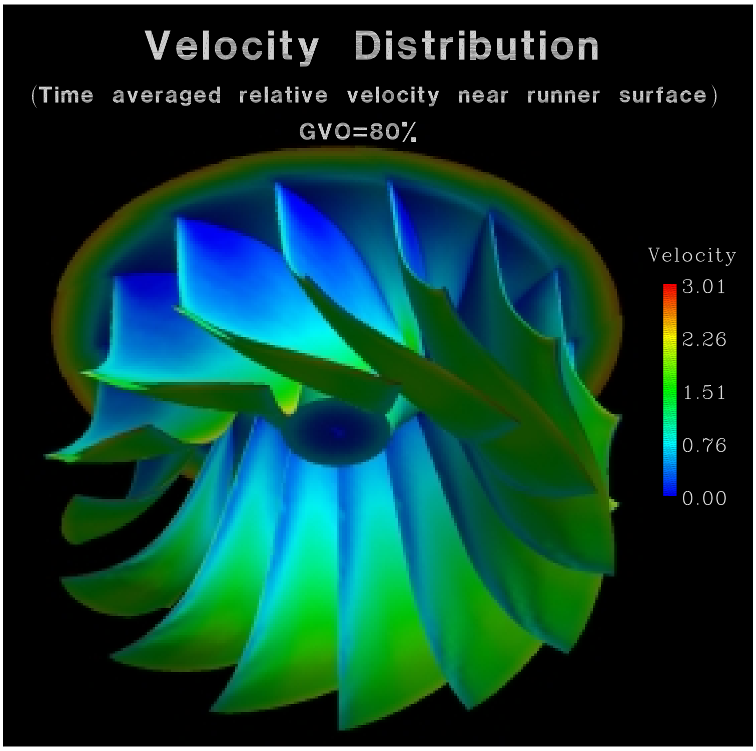


(a)

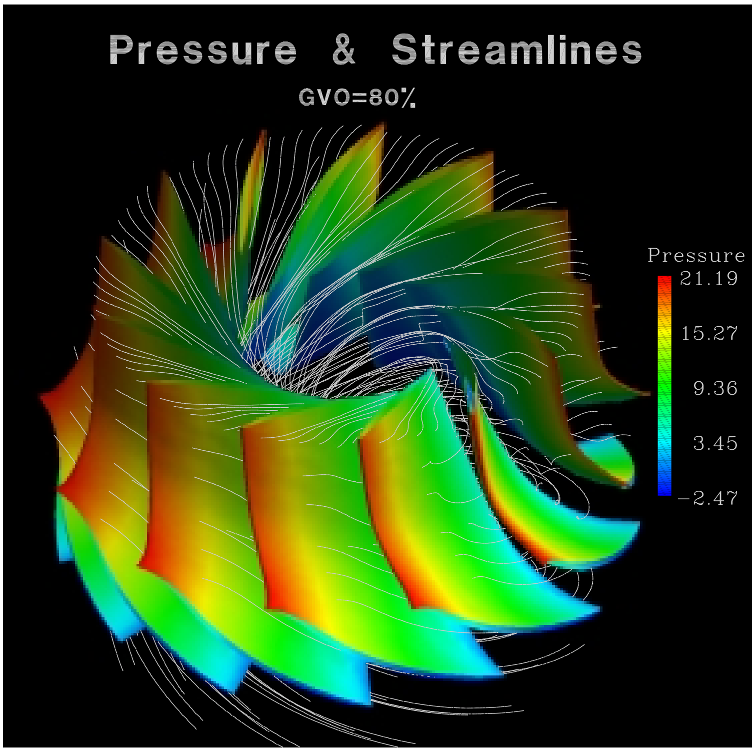


(b)

Fig.6: Time-averaged relative velocity and pressure distributions:
(a) Velocity magnitude distrubution and (b) Surface pressure and streamlines